Benchmark Simulations of Rotor Aerodynamics on the IEA Wind 15MW RWT and Associated Modeling Challenges

Benchmark Simulations of Rotor Aerodynamics on the IEA Wind 15MW RWT and Associated Modeling Challenges

K Boorsma[1], J G Schepers[1], G R Pirrung[2], H A Madsen[2], N N Sørensen[2], C Grinderslev[2], M Imiela[3], F Krimm [3], G Bangga[4], W Gonçalves Pinto[5], L Greco[6], C Testa[6], J Theron[7], L Höning[7], J Jonkman[8], E Branlard[15], M Chetan[8], R Boisard[9], A Croce[10], S Cacciola[10], S Cherubini[11], N Aryan[12], H Asmuth[13], L Pagamonci[14], F Papi[14] and A Bianchini[14]

[1]TNO, Petten, The Netherlands
[2]DTU, Roskilde, Denmark
[3]DLR, Braunschweig, Germany
[4]DNV, Bristol, UK
[5]IFPEN, Rueil-Malmaison, France
[6]CNR-INM, Rome, Italy
[7]IWES Fraunhofer, Bremerhaven, Germany
[8]NLR, Colorado, USA
[9]ONERA, Paris, France
[10]POLIMI, Milano, Italy
[11]POLIBA, Bari, Italy
[12]Sapienza, Rome, Italy
[13]Uppsala, Uppsala, Sweden
[14]Unifi, Firenze, Italy
[15]UMass-Amherst, Massachusetts, USA

E-mail: koen.boorsma@tno.nl

Abstract. A large comparison exercise has been performed featuring aerodynamic and aero-elastic simulation cases on the IEA 15MW reference wind turbine in various conditions, containing results of 30 codes ranging from BEM to CFD. More than 10 different variable types ranging from lifting line variables to pressures, loads and velocities have been compared for the different conditions, resulting in many comparison plots. The result is a unique insight in the current status and accuracy of rotor aerodynamic modeling. Although there are no measurements on this turbine, mutual comparison of model results provided useful insights into the performance of rotor aerodynamic models.
Preparatory simulations on the 15MW RWT at constant uniform conditions generally showed reasonable agreement in the aerodynamic response between engineering and higher-fidelity models, provided the turbine was considered rigid. However, including flexibility effects led to more discrepancies, largely due to differences in blade torsion, which in turn impacts the aerodynamics. Even at

very moderate wind speeds the blade tip torsion angle could be in the order of 2 degrees where large differences were found between the partners results.
Following the preparatory cases, simulations under turbulent conditions were performed. Several turbulent boxes were generated using high-fidelity CFD models and the results were compared mutually. Some differences appeared in the turbulent boxes, which could be expected from convection differences. At first sight the differences seemed small. However, when the boxes were fed into an aeroelastic code, the differences became significant enough to affect load response. When supplying the sampled wind speeds from the turbulent box as input to engineering-fidelity models, it was interesting to find that these models showed a much higher standard deviation in loads compared to higher-fidelity models. This confirms the finding from previous numerical studies that engineering models tend to overpredict fatigue loads, also for a large sized rotor.

1. Introduction

Within the framework of International Energy Agency (IEA) Wind TCP Task 47 TURBINIA [1], a large international consortium representing research and industry bodies cooperates to assess and improve the accuracy of rotor aerodynamic simulation models. Although these models are used to design wind turbines, they often show major shortcomings that can result in inefficient and unsafe operation. A long-lasting effort of IEA Tasks, initiated in the 1990s, has preceded the current Task [2–8]. Historically, experimental data from the field and wind tunnel have been used to provide a means of validation [9–11]. After the most recent comparison rounds that subjected the DanAero experiment [12, 13], the focus shifted to the modeling challenges of large wind turbines, more representative of today's market. Unfortunately, public measurements on large-scale turbines including sufficiently detailed instrumentation are scarce, motivating our current comparison between low- and high-fidelity models. Several participants of TURBINIA performed simulations with a variety of aerodynamic codes (both Computational Fluid Dynamics - CFD - and lifting line - LL - codes) subjecting the IEA 15MW reference wind turbine [14], which features a 242 m diameter rotor. The results from the calculations were compared mutually. The first comparison round has been performed for constant, axial flow and can be considered a preparatory case to ensure consistent modeling in terms of input and output. After this round the focus shifted to a case featuring turbulent inflow. This paper presents a more concise version of the results of these comparison rounds, which are also reported in the technical report of IEA Task 47 [1].

2. Preparatory Case: Constant, axial flow

Two cases are defined as summarized in Table 1, purposely selecting an operational point around design conditions in partial load. For one simulation the turbine is modeled flexible, for the other one, tower, rotor etc. are modeled rigidly. For the lifting line codes, airfoil data are prescribed including a 3D correction based on the method of Snel[15]. The blade geometry is prescribed by an IGES file, plus the availability of common mesh files, to promote uniformity for the blade resolved CFD simulations. The participants are summarized in Table 2, contributing by using a variety of rotor aerodynamic models ranging in fidelity from BEM to blade-resolved CFD.

Figure 1 shows the spanwise variation of chordnormal force values. These are non-dimensionalized using undisturbed local dynamic pressure (determined from wind and local rotational speed) to allow for a solid comparison between simulation results along the span without the complications

Table 1. IEA 15MW comparison cases

Case nr	Model config‡	Wind speed U_∞ [m/s]	Turb. intensity TI [%]	Pitch angle [°]	Rot. speed ω [rpm]	Tip speed ratio λ [-]	Angle of attack $\alpha^\dagger$@80%R [°]	Axial ind. factor $a^\dagger$@80%R [-]
V2.1	Rigid	7.5	0	0.0	5.33	8.9	7.5	0.32
V2.2	Flexible	7.5	0	0.0	5.33	8.9	6.0	0.27
V2.3	Rigid	7.5	~8	0.0	5.33	8.9	7.5	0.32

‡ Tilt, cone and yaw angles are set to zero, but blade prebend is included. The tower shadow effect is disregarded.
† Estimate using a BEM simulation

Table 2. High-level summary of participant codes and settings.

Legend Entry	Participant	Code Name	Aero Model†	Struc. Model
Bladed_BEM	DNV	Bladed	BEM	multi-body
Bladed_VL	DNV	Bladed	LL-FVW	multi-body
DLR_SPCK_TAU	DLR	Tau	RANS	rigid
DLR_SPCK_AD	DLR	SIMPACK-AD	BEM (AeroDyn)	multi-body
DTU_EllipSys3D	DTU	EllipSys3D	RANS	multi-body
DTU_HAWC2	DTU	HAWC2	BEM	multi-body
DTU_HAWC2NW	DTU	HAWC2	BEM plus nearwake	multi-body
DTU_HAWC2NWVC	DTU	HAWC2	NW plus vortex cylinder	multi-body
IFPEN_BEM	IFPEN	DeepLines Wind	BEM *(AeroDeeP)*	multi-body
IFPEN_VL	IFPEN	DeepLines Wind	LL-FVW *(CASTOR)*	multi-body
INM_Aeolian	CNR-INM	Aeolian	BEM	multi-body
INM_FunAero	CNR-INM	FunAero	Panel code	rigid
IWES_BD_BEM	IWES	OpenFAST	BEM (AeroDyn)	multi-body
IWES_BD_OLAF	IWES	OpenFAST	LL-FVW (OLAF)	multi-body
IWES_OpenFOAM	IWES	OpenFOAM	RANS	rigid
NLR_ED_BEM	NLR	OpenFAST	BEM (AeroDyn)	modal
NLR_ED_OLAF	NLR	OpenFAST	LL-FVW (OLAF)	modal
NLR_BD_BEM	NLR	OpenFAST	BEM (AeroDyn)	multi-body
ONERA_FAST	ONERA	FAST	URANS-AL	rigid
ONERA_PUMA	ONERA	PUMA	LL-FVW	rigid
TNOAero_ED_BEM	TNO	AeroModule	BEM	modal
TNOAero_ED_AWSM	TNO	AeroModule	LL-FVW (AWSM)	modal
TNOAero-BEM-S	TNO	AeroModule	BEM (240° sector)	rigid
PhatAero-BEM	TNO	AeroModule	BEM	multi-body
TNO_OpenFOAM	TNO	OpenFOAM	RANS	rigid
PoliBa_LES	Politecnico Bari	-	LES-AL	rigid
PoliMi_Cp-Lambda	PoliMi	Cp-Lambda	BEM	multi-body
Sapienza_AL	Sapienza Rome	OpenFOAM	RANS-AL	1D-FEM
Unifi_ALM	Uni di Firenze	Converge CFD	LES-AL	modal
UU_ALM	Uppsala Uni	OpenFOAM	LES-AL	modal

† BEM: Blade Element Momentum, LL-FVW: Lifting Line Free Vortex Wake, AL: Actuator Line, (U)RANS: (Unsteady) Reynolds Averaged Navier-Stokes, LES: Large Eddy Simulation

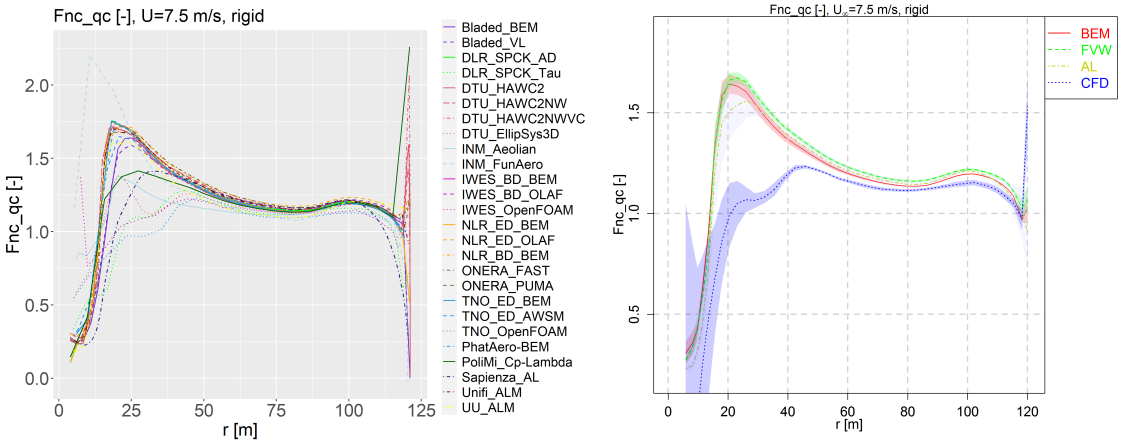

Figure 1. Comparison of non-dimensionalized chordnormal force distribution for all participants (left) and averaged per model type (right), rigid case. For the model averaged results, the band illustrates the variability of the results for each code type by means of the standard error.

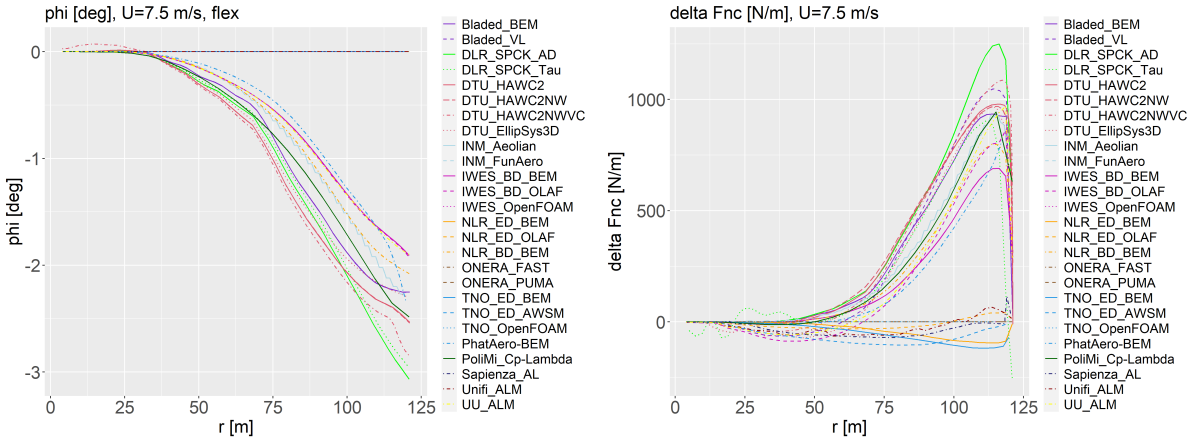

Figure 2. Comparison of predicted torsion angle distribution (left) and difference in normal force between rigid and flexible simulation (right).

of uncertainty in rotor induced velocities. To aid the interpretation of the plots with individual code results, BEM, FVW and CFD results feature a solid, dashed and dotted line respectively. The inboard area exhibits large angles of attack and three-dimensional separated flow features, which cause deviations between lifting line methods and rotor resolved CFD results (and between CFD results themselves). Confirming this observation, the right hand side plot shows average and a band illustrating the variability of the results for each code type. Besides these differences, there is a generally good agreement between the different codes. For more results, the reader is referred to the final report of this Task [1], which features a comparison of pressure distribution, sectional forces and lifting line variables.

The effect of flexibility is dominated by torsional deformation, which shows a considerable modeling spread as illustrated in the left hand side plot of Figure 2. A further study into the effect of different structural models for this case is given in the final report [1]. The difference in normal force between the rigid and flexible situation (right hand side plot) is clearly dominated by the torsion angle and whether this degree of freedom is included in the modeling, resulting in values above zero. A closer look at the difference between rigid and flexible simulations also

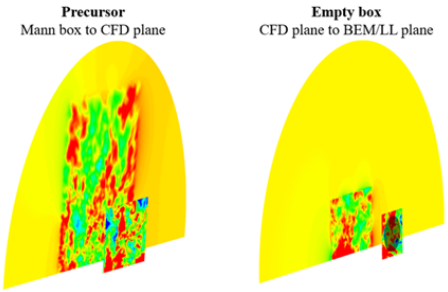

Figure 3. Illustration of inflow generation procedure. Left: Mann input sampled for CFD runs after 200m. Right: Empty box simulation with CFD planes imposed 300m upstream and new planes sampled at the rotor plane.

Size	4096×1024×1024 m
Points	1024×256×256
Ae-factor	1
Gamma	3
L	90.0 m
Scale-factor	0.2

Table 3. Mann box input settings

reveals a non-negligible effect in the inboard region for the dashed and dash-dotted FVW and AL results, which does not exist for the BEM results that feature a solid line type. This difference is attributed to the displacement of the tip in the flexible situation. This shift of the wake position has an influence on the axial induced velocity, which is then also noticeable in the inboard part, even though the inboard deflections are extremely small.

3. Second round: Turbulent inflow

After achieving consistency in the model set-up for the IEA15MW reference wind turbine, illustrated by the outcome of preparatory cases in section 2, a more challenging test case was pursued. A turbulent inflow round was defined featuring the IEA 15MW reference wind turbine. The time averaged conditions of this round are identical to the constant uniform inflow case, summarized as Case V2.3 in Table 1. A turbulent wind field without vertical wind shear has been created, which results in a turbulence intensity of around 8% at the rotor plane. As the primary focus is on the differences in aerodynamic modeling, the rotor is modeled rigid.

3.1. Inflow generation

From IEA Wind Task 29 [8], experience was gained in imposing turbulence inside CFD domains and convecting these downstream towards the rotor, and comparing the CFD predicted loads to results from lifting line codes that impose the turbulence at the rotor plane. This resulted in good matching of average loads between the code types [13]. For this specific task, a few adjustments are done to hopefully obtain even better agreement between codes. It was decided to use a precursor CFD simulation, fed by input from a Mann-box generator, to act as an initial filter ensuring a better match in the turbulent inflow seen at the rotor across the codes. Therefore, two turbulence planes were prescribed: one for CFD to be imposed 300 m upstream, and then one from each CFD code extracted in an empty box simulation for the LL/BEM codes to be imposed at the rotor plane position. By doing so, the discrepancies due to the flow development between the imposed plane and the rotor are minimized.

3.1.1. Plane creation A turbulence box has been created using Mann box generated inflow, which is then filtered through a CFD simulation (precursor), in order to make the box more CFD-friendly. The Mann box was created with the input according to Table 3 and scaled to TI of 12.6% (mean overall) before being inputted to the CFD precursor run. This box was then inserted to an empty CFD domain 500 m upstream of the rotor position. New planes were sam-

pled 300 m upstream of the rotor position (so after 200 m convection from input plane) for CFD simulations. The TI of the CFD input plane (averaged in space and time) is 9.6%, resulting in a drop of 3 percent points from the Mann box to the precursor sampling. As mentioned above, the TI decreases further from the CFD input plane to the rotor plane, resulting in an average TI of approximately 8% at the rotor plane, depending on the CFD code used and its settings. See also Figure 3 for an illustration of the above outlined process.

3.1.2. Inflow differences and effect on loads

Subsequently, several high fidelity CFD models (CFD entries from DTU, UNIFI, DLR and ONERA as highlighted in Table 2) were used to generate empty turbulent boxes and the results were compared mutually. Hereto the statistics were sampled over a duration of approximately 200 s. At first sight, the differences seemed small, as illustrated in Figure 4. Although good agreement exists between the mean levels, notable differences are apparent in terms of standard deviation. To verify to what extent the variations in the flow field affect the loads, the TNOAero-

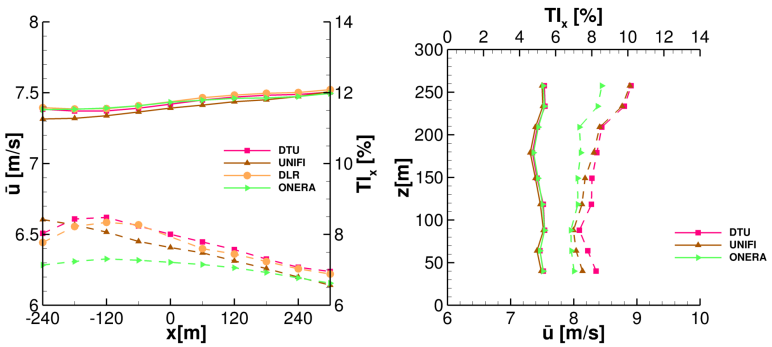

Figure 4. Profiles of mean streamwise velocity and turbulent intensity for empty box results from different CFD simulations. Means in solid and TI in dashed lines. Left shows longitudinal profiles at hub height (148 m), right shows vertical profile at the axial position of the rotor plane (x=0).

BEM code is fed with the different inflow fields. Unfortunately it was not possible to export the DLR generated inflow field for feeding to this BEM code. However, results from PoliBa inflow fields were added, despite the fact that post-processed empty box profiles as shown in Figure 4 were not available from this code. Figure 5 gives an overview of the resulting flapwise blade root moment statistics (aerodynamic contributions only), in relation to the hub height wind speed. Here it can be observed that, similar to the empty box comparison, there is a good agreement

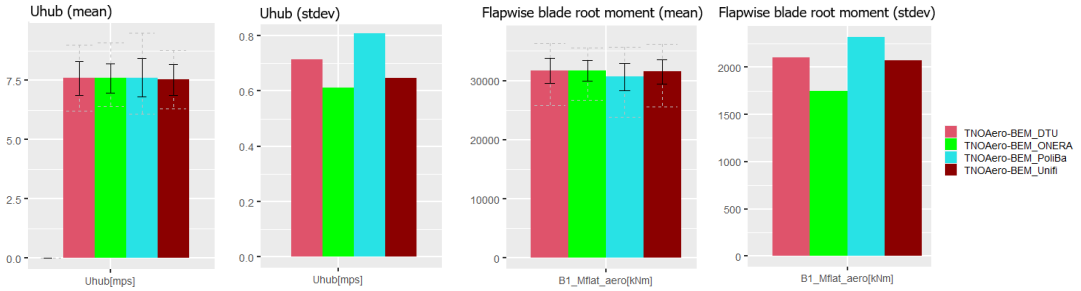

Figure 5. Mean and standard deviation of hub height wind speed (left) and flapwise blade root moment (right) for different CFD calculated empty box inflow fields fed to the same BEM code. For the mean bar plots, min and max are indicated in grey, and standard deviation in black).

of the mean levels, but there is a considerable difference in the unsteady content. For example there is more than 30% difference between the highest and lowest standard deviation of the flapwise blade root moment. The agreement in trends between the standard deviation of the hub height wind speed and flapwise blade root moment is striking. From this exercise we can conclude that care should be taken when comparing rotor CFD results between each other, as the differences in loads could well be attributed by convection differences (i.e. a different inflow field at the rotor plane) instead of differences in the rotor aerodynamic modeling. Therefore it was decided to enforce an identical empty box inflow field for the lifting line simulations, which in this case was the inflow field determined from the EllipSys3D simulation provided by DTU.

3.2. Rotor aerodynamic modeling

As mentioned, planes from empty box CFD simulations, sampled at the rotor plane position, should be used for the lifting line simulations. To be able to compare the lifting line results to rotor CFD simulations, the time delay due to the different starting point 300 m upstream instead of the rotor plane for the lifting line simulations needs to be accounted for. In addition to a simple convection at the freestream wind speed of 7.5 m/s, the additional time delay due to rotor blockage needs to be taken into account. To determine the magnitude of this delay, several methods can be used such as cross correlation between empty box and rotor simulation results [16]. In reality the magnitude of this delay is subject to spatial variation across the rotor plane since the induction is distributed non-uniformly. For the current project, the approach taken is to use CFD results from a uniform inflow simulation and determine a spanwise average of the induction at the different upstream stations. An additional delay was determined by integrating this wind speed over the region between 300 m upstream and the rotorplane.

To monitor the spanwise variation of variables, virtual probes are defined at four different radial location along the first blade (25%, 44%, 64% and 85% span, denoted by r1 to r4). To facilitate interpretation, plots with time traces, statistics based on the time traces (min, max, mean, stdev), bin azimuthal averages and power spectral densities (PSDs) are generated. After confirming the inflow prescription to be consistent between lifting line and CFD codes, the sectional loads are studied in Figure 6 by means of the chordnormal force. Similar to previous studies [13, 17], the mean load levels are in good agreement but a consistent drop in standard deviation appears from BEM to FVW codes for all radial stations. A closer look reveals that the CFD results (including the DTU EllipSys3D results of which the empty box was used to feed the inflow for the lifting line codes) are also featuring lower standard deviation levels, more in line with the FVW results. To shed some light on the cause for the differences between BEM and FVW codes, the local axial induced velocity variations (at the position of the element as used in the velocity triangle of the lifting line simulations) were studied in Figure 7. Here it can be identified that most FVW codes (dashed lines) feature a more direct response to incoming velocity variations, which is partly attributed to the shed vorticity effect impacting the high frequency content, but also due to a different response to the slower 1P variations which dominate the unsteady loading characteristics. Based on the results, it could be anticipated that, depending on the BEM code implementation, design calculations for certification using this code type could over predict fatigue loading for individual cases by more than 10%. Interestingly, experimental validation by industry partners in the task has not backed up this observation. Furthermore, scoping analyses for an entire fatigue load set have previously estimated the overall fatigue difference to around 5%. This is a consequence of the relatively large contribution of the higher wind speeds to the overall fatigue, for which the induction effect and hence the over prediction are much lower [17].

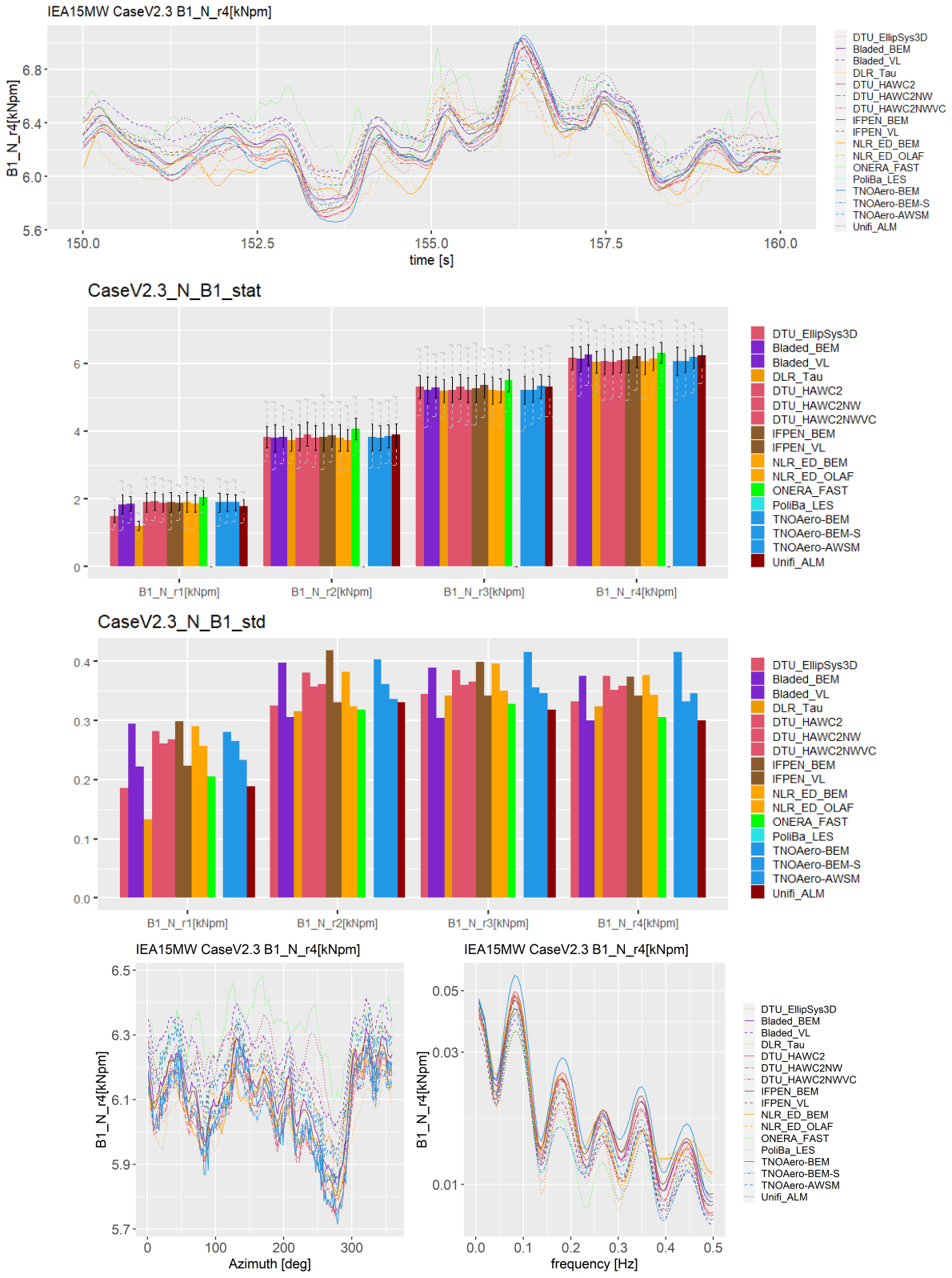

Figure 6. Normal force for the Case V2.3 rotor simulations. Top (time traces, r4), middle top (bar mean, r1 to r4 with min and max in grey and stdev in black), middle bottom (bar standard deviations, r1 to r4), bottom left (bin azimuth averages, r4) and bottom right (PSD, r4). The order of the bars corresponds to the order of the legend entries.

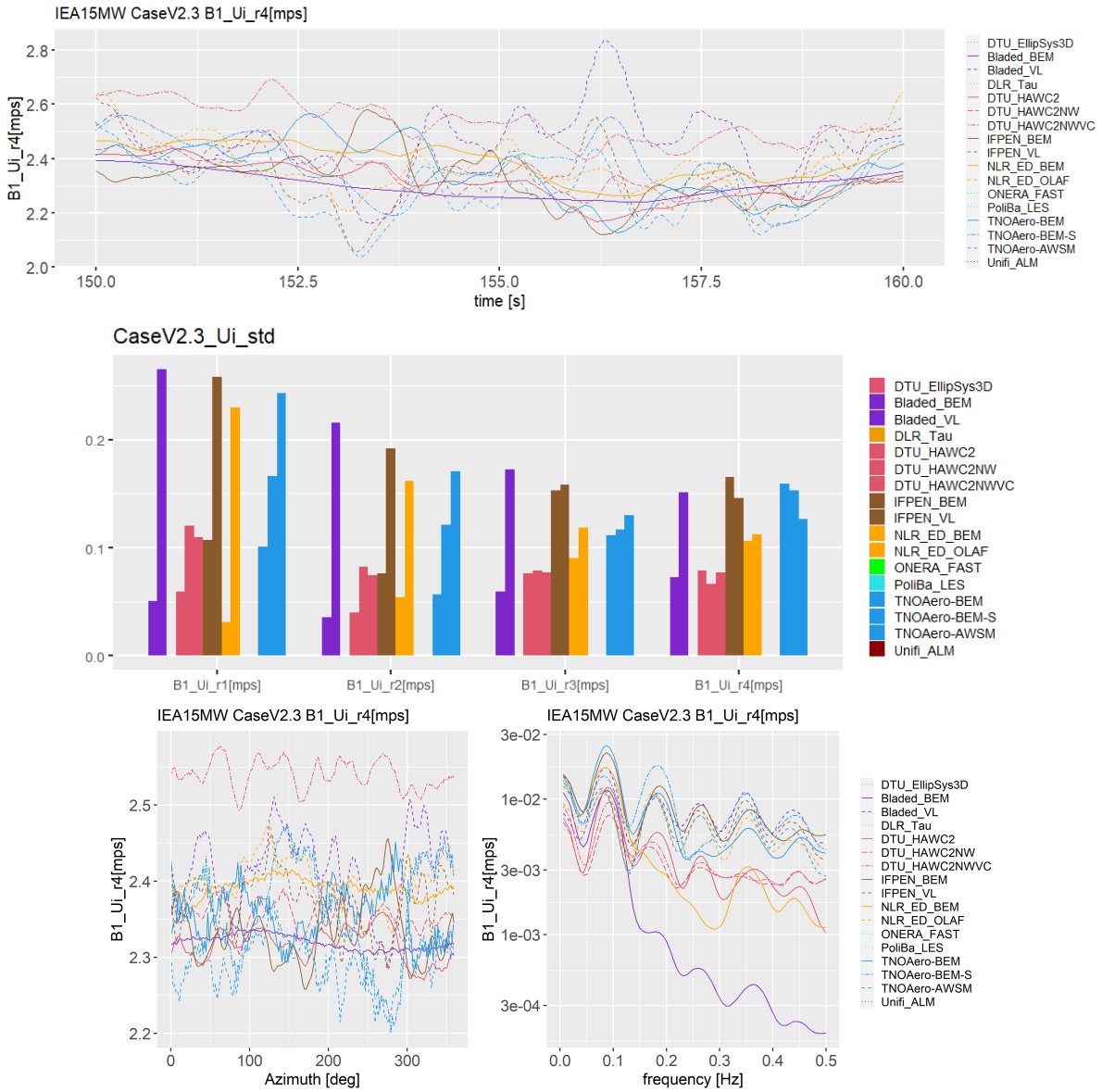

Figure 7. Local axial induced velocity for the Case V2.3 rotor simulations. Top (time traces, r4), middle (standard deviations, r1 to r4), bottom left (bin azimuth averages, r4) and bottom right (PSD, r4). The order of the bars corresponds to the order of the legend entries.

4. Conclusions and recommendations

A large comparison exercise has been performed featuring aerodynamic and aero-elastic simulation cases on the IEA 15MW reference wind turbine in various conditions, containing results of 30 codes ranging from BEM to CFD. Although there are no measurements on this turbine, mutual comparison of model results provided useful insights into the performance of aerodynamic models.

Preparatory simulations at constant uniform conditions in partial load generally showed reasonable agreement in the aerodynamic loads between engineering and higher-fidelity models considering a rigid turbine. However, significant discrepancies were observed in the predicted blade torsion angle up to 2 degrees, consequently resulting in a load offset between these models.

Despite the challenges in aligning CFD and lifting line codes in turbulent inflow, a methodology was devised to perform a successful comparison for these conditions. In agreement with previous studies, it was found that the engineering fidelity BEM models significantly overpredict standard deviation of sectional aerodynamic loads compared to higher fidelity models, now also for a large sized rotor. Acknowledging BEM is the industry standard, it is recommended to further investigate this finding by means of a detailed code validation exercise together with industry. Furthermore it is stressed once again that continuing these benchmarks in the wind community is important, especially in combination with detailed aerodynamic measurement data for validation, to progress on the subjected topics and reduce the large uncertainty that still persists in unsteady rotor aerodynamic modeling.

Acknowledgements

The authors would like to thank IEA TCP Wind for facilitating the TURBINIA project in their framework. The contributions of the participants to TURBINIA have been funded in various national programmes, which are detailed in the corresponding final report [1]. This work was authored in part by the National Laboratory of the Rockies for the U.S. Department of Energy (DOE), operated under Contract No. DE-AC36-08GO28308. Funding for this contribution was provided by the U.S. Department of Energy Office of Critical Minerals and Energy Innovation Wind Energy Technologies Office. The views expressed in the article do not necessarily represent the views of the DOE or the U.S. Government. The U.S. Government retains and the publisher, by accepting the article for publication, acknowledges that the U.S. Government retains a nonexclusive, paid-up, irrevocable, worldwide license to publish or reproduce the published form of this work, or allow others to do so, for U.S. Government purposes.

References

[1] Schepers J *et al.* 2025 IEA Wind TCP Task 47, TURBINIA, Turbulent Inflow Innovative Aerodynamics, Final Technical Report, Phase I Tech. rep. URL https://doi.org/10.5281/zenodo.17897185

[2] Schepers J *et al.* 1997 Final Report of IEA Annex XIV: Field Rotor Aerodynamics Tech. rep. ECN-C–97-027

[3] Schepers J *et al.* 2002 Final report of IEA Annex XVIII' Enhanced Field Rotor Aerodynamics Database ECN-C-02-016 Energy Research Centre of the Netherlands, ECN

[4] Schreck S 2008 IEA Wind Annex XX: HAWT Aerodynamics and Models from Wind Tunnel Measurements NREL/TP-500-43508 The National Renewable Energy Laboratory, NREL

[5] Schepers J *et al.* 2012 Final report of IEA Task 29, Mexnext (Phase 1): Analysis of MEXICO wind tunnel measurements ECN-E-12-004 Energy Research Center of the Netherlands URL https://publications.tno.nl/publication/34629143/5lE9u6/e12004.pdf

[6] Boorsma K *et al.* 2014 Final report of IEA Task 29, Mexnext (Phase 2): Analysis of MEXICO wind tunnel measurements ECN-E-14-060 Energy Research Center of the Netherlands URL https://www.ecn.nl/publications/ECN-E-14-060

[7] Boorsma K *et al.* 2018 Final report of IEA Task 29, Mexnext (Phase 3): Analysis of MEXICO wind tunnel measurements ECN-E-18-003 Energy Research Center of the Netherlands URL https://publications.tno.nl/publication/34629481/463fjb/e18003.pdf

[8] Schepers J *et al.* 2021 Final report of Task 29, Phase IV: Detailed Aerodynamics of Wind Turbines Tech. rep. URL https://doi.org/10.5281/zenodo.4925963

[9] Hand M *et al.* 2001 Unsteady Aerodynamics Experiment Phase VI Wind Tunnel Test Configurations and Available Data Campaigns NREL/TP-500-29955 National Renewable Energy Laboratory, NREL

[10] Schepers J and Snel H 2007 MEXICO, Model experiments in controlled conditions ECN-E-07-042 Energy Research Center of the Netherlands

[11] Bak C *et al.* 2013 DANAERO MW: Instrumentation of the NM80 turbine and meteorology mast at Tjæreborg Report-I-0083 DTU Wind Energy

[12] Boorsma K *et al.* 2023 Progress in the validation of rotor aerodynamic codes using field data *Wind Energy Science* **8** 211–230 URL https://wes.copernicus.org/articles/8/211/2023/

[13] Boorsma K *et al.* 2024 Challenges in rotor aerodynamic modeling for non-uniform inflow conditions *The Science of Making Torque from Wind (TORQUE 2024)* (Florence, Italy: IOP Publishing) p 022006 URL https://iopscience.iop.org/article/10.1088/1742-6596/2767/2/022006

[14] Gaertner E *et al.* 2020 Definition of the IEA 15-Megawatt Offshore Reference Wind Tech. Rep. NREL/TP-5000-75698 National Renewable Energy Laboratory

[15] Snel H, Houwink R, van Bussel G and Bruining A 1993 Sectional prediction of 3d effects for stalled flow on rotating blades and comparison with measurements *Proc. European Community Wind Energy Conference*

[16] Wenz F *et al.* 2020 Cross-correlation-based approach to align turbulent inflow between cfd and lower-fidelity-codes in wind turbine simulations *Journal of Physics: Conference Series* vol 1618 (IOP Publishing) p 062005

[17] Boorsma K *et al.* 2020 Validation and accommodation of vortex wake codes for wind turbine design load calculations *Wind Energy Science* **5** 699–719 URL https://wes.copernicus.org/articles/5/699/2020/